Dear editor,

We thank you again for the good suggestions and terminology corrections. Please see our reply below.

Associate Editor Decision: Publish subject to minor revisions (further review by editor) (17 Nov 2020) by Axel Gerdes

Comments to the Author:

Dear Perach Nurial et al.,

many thanks for sending the revised ms. The modifications you did are in line with the reviewers suggestions... However, there is one thing which gets more confusing through the changes. It is the distinction between single and multi-collector ICPMS ... as you aim to discuss the point that ASH15 appears not to be a suitable RM for single-collector but for MC-ICP-MS... (section 4.5)

What is the basis of it? You mentioned before acquired single- and multi-collector data on ASH-15 in different labs and showed this in a figure, but not discussed differences of the data sets. Perhaps you can do it or don't want to do?

However, other labs acquired reasonable single collector ASH15 data: Frankfurt lab published various papers (e.g. Scardia et al. 2019 QSR, Cruset et al. 2020 J Geol Soc London, and Marine Petrol Geol 120) in which we used ASH15 and yielded precise ages (+-2%), within the uncertainty of the published ASH15 data. The same applies to Guillong et al. 2020 (this Spec. volume) … within 2% (excess of variance). At least there is currently no proof that LA MC-ICPMS data is much better than LA SC-ICPMS data.

It becomes a bit more confusing the section 4.5. The text partly speaks of sector-field ICPMS instead of MC-ICPMS, elsewhere it seems that Sectorfeld = MC-ICPMS is used, and for single-collectors "including Q-ICPMS" is added. It seems that the authors did not want to commit themselves or have made some changes based on the reviewer's comments, but not applied this consistent throughout the text. So the unexperient reader still gets the impression that compared with MC-ICPMS, single collector is not suitable for ASH15 analyses. While experient reader might come to the conclusion that the authors are confused and want to make a statement towards MC-ICPMS..

The main controlling factor is simply sensitivity or better signal strength (=depending on concentration and spot size and instruments sensitivity). Sector-field (single- and multi-collector !!!) are more sensitive than quadropole ICP-MS. Multicollector ICPMS are usually more sensitive than single-collector SF-ICPMS. However, if you consider older generation of MC-ICPMS and the MC-ICPMS from one company compared to that from another company (Neptune higher sensitivity than Nu Plasma; Element XR > Attom) , it stays true only in relative terms. The same applies to the older Element2 versus the ElementXR with Jet-interface.

So I would suggest that you change the text in section 4.5, and use instead a term like (line 424) less-sensitive ICP-MS (e.g. most quadrupole ICP-MS) and more-sensitive ICPMS (e.g. new generation of single and multi-collector ICPMS) for text line 427. And "Finally the JT …. can be used for most single- and multi-collector sector-field ICPMS instrument as well as the newer generation of quadrupole ICPMS.

Answer: we apologies for the confusing terminology and we have changed it as suggested to 'less-sensitive ICP-MS (e.g. most quadrupole ICP-MS)' and 'more-sensitive ICPMS (e.g. new generation of single and multi-collector ICPMS)'

- Please check the text again for typos/spelling, I found 3 times "available" (line 288, 307, 319). Avilable

Thanks, corrected!

- Fig 4b (BGC) What stands this for BGS? Please change and explain it in the text.

Corrected to BGS for 'British Geological Survey' and also also explained in figure caption.

- Line 330 primary MS ??? you mean primary RM

Corrected to RM (reference material)

- you consistent single-collector and multi-collector... in the text you write as well single collector ICP

Thanks, we have changed to single-collector and multi-collector throughout the text

Best wishes Axel Gerdes

1 **The use of ASH-15 flowstone as a matrix-matched reference material for laser-ablation**

2 **U-Pb geochronology of calcite**

3 Perach Nuriel[1], Jörn-Frederik Wotzlaw[2], Maria Ovtcharova[3], Anton Vaks[1], Ciprian Stremtan[4],

4 Martin Šala[5], Nick M. W. Roberts[6], and Andrew R. C. Kylander-Clark[7]

6 [1] Geological Survey of Israel, 32 Yeshayahu Leibowitz St. Jerusalem, 9692100, Israel

7 [2] Institute of Geochemistry and Petrology, ETH Zurich, Clausiusstrasse 25 I CH-8092 Zurich,

8 Switzerland

9 [3] Department of Earth Sciences, University of Geneva, Geneva, Switzerland

10 [4] Teledyne Photon Machines, 384 Gallatin Park Drive, Bozeman, MT 59715, USA

11 [5] Department of Analytical Chemistry, National Institute of Chemistry, Hajdrihova 19, SI-1000

12 Ljubljana, Slovenia.

13 [6] Geochronology and Tracers Facility, British Geological Survey, Environmental Science

14 Centre, Nottingham, NG12 5GG, UK

15 [7] Department of Earth Science, University of California, Santa Barbara, CA 93106, USA.

17 **Abstract**

18 Latest advances in laser ablation inductively coupled plasma mass spectrometer (LA-ICPMS)

19 allow for accurate *in-situ* U-Pb dating of carbonate material, with final age uncertainties usually

20 >3% 2σ. Cross-laboratory reference materials (RMs) used for sample-bracketing are currently

21 limited to WC1 calcite with an age of 254.4 ± 6.5 (2σ). The minimum uncertainty on any age

22 determination with the LA-ICPMS method is therefore ≥ 2.5%, and validation by secondary

23 RMs ~~are~~ is usually performed on in-house standards. This contribution present a new reference

24 material, ASH-15, a flowstone that is dated here by ~~i~~Isotope ~~d~~Dilution (ID) TIMS analysis

25 using ~~36~~ 37 sub-samples, 1-7 mg each. Age results presented here are slightly younger

26 compared to previous ID-IRMS U-Pb dating dates of ASH-15, but within uncertainties and in

27 agreement with *in-situ* analyses (using WC1 as the primarya RM). We provide new correction

28 parameters to be used as primary or secondary standardization. The suggested ^{238}U/^{206}Pb

29 apparent age, not corrected for disequilibrium and without common-lead anchoring, is 2.965 ±

30 0.011 Ma (uncertainties are 95% confidence intervals2σ). The new results could improve the

31 propagated uncertainties on the final age with a minimal value of 0.4%, which is approaching

32 the uncertainty of typical ID analysis on higher-U materials, for example, such as zircon (<1%

33 2s). We show that although LA-ICPMS spot analyses of ASH-15 exhibits significant scatter in

34 their isotopic ratios, the down-hole fractionation of ASH-15 is similar to that of other reference

35 materials. This high-U (~1 ppm) and low Pb (<0.01 ppm) calcite is most appropriate as a

36 reference material for other speleothem-type carbonates but requires more-sensitive ICP-MS

37 instruments such as the new generation of single-collector and multi-collector ICP-MSsensitive

38 sector-field ICP-MS instruments. Reference materials with high Pb and low U or both low U

39 and Pb compositions are still needed to fully cover the compositional range of carbonate

40 material but may introduce analytical challenges. For LA work, we recommend the use of the

41 new ID-TIMS ages that are 1.3-1.5% younger than previously suggested, because of the lower

42 uncertainties (0.4%), the large number of sub-samples (n=36), the use of the EARTHTIME

43 isotopic tracers, and the small aliquots (1-7 mg) that are more representative of laser-ablation

44 spot analysis.

45

Introduction

47 Recent advances in laser ablation techniques applied to multi-phase carbonates allow for

48 accurate dating of a variety of sample types, including calcite cements (Li et al., 2014; Godeau

49 et al., 2018; Anjiang et al., 2019; Holdsworth et al., 2019), hydrothermal veins (Coogan et al.,

2016; MacDonald et al., 2019; Piccione et al., 2019), fault-related veins, breccia cement, and slickenfibers (Ring and Gerdes, 2016; Roberts and Walker, 2016; Goodfellow et al., 2017; Nuriel et al., 2017; Hansman et al., 2018; Parrish et al., 2018; Nuriel et al., 2019), and speleothems (Woodhead and Petrus, 2019). With increasing attention ~~on~~ to climatic, seismic, and environmental events in the geological record, there is a growing need for dating techniques that can be accurate~~ly~~ and easily implemented ~~to~~ for samples at the sub-millimeter scale. This newly emerging technique has the potential to contribute to our understanding of the duration, rate, and extent of these important events in the geological record.

The *in-situ* approach has a great research potential for studying texturally complex samples because it can resolve problems of age mixing of different phases or averaging of continuous growth at the sub-millimeter scale, and thus increase the overall accuracy of the dated material. While the precision of traditional isotope-dilution (ID) U-Pb analyses is still favorable (<1% 2σ) (Woodhead and Petrus, 2019), the increasing analytical development of the LA-ICPMS method indicates the potential for improving the currently reported uncertainties (usually >3% 2σ). Finding the right matrix-matched reference material (RM) is a major hurdle for LA analyses of carbonates because of the variety of mineralogy (calcite, dolomite, and aragonite), textures, composition (e.g. high-magnesium calcite, high common-lead), and ages (e.g. low radiogenic lead in young samples). Textural differences such as microcrystalline, fine- and coarse-grained material, between the unknown and RMs can contribute to high uncertainties due to differences in ablation efficiency, down-hole fractionation, and differences in crater morphology (e.g. Guillong et al., 2020 and Elisha et al, 2020, this issue). Observed deviations are potentially up to 20% of the final intercept age depending on the degree of crater geometry mismatch and are related ~~to~~ either to downhole fractionation and/or matrix effects (Guillong et al., 2020).

74   Currently, the most commonly used procedure for mass-bias correction in the LA method, is

75   by standard-sample bracketing. For this, the ^{238}U/^{206}Pb LA-age of the RMs is corrected to the

76   true RM's ^{238}U/^{206}Pb apparent age (not corrected for disequilibrium) as measured

77   independently by an ID-IRMS method (e.g. ID-TIMS or ID-MC-ICPMS). The RMs are

78   measured throughout each session along with the unknown samples, and a normalization factor

79   is applied to correct both the RMs and the unknowns. Uncertainty propagation onto the age of

80   the unknowns includes the uncertainties of the 'true' RM age. As a result, the accuracy of the

81   LA analyses can only be as good as the uncertainties on the age of the RMs which is by itself

82   subjected to analytical challenges due to natural heterogeneities, impurities, and textural

83   complexities at the sub-millimetre scale. It is therefore essential that the 'true age' of the

84   reference material will reflect these complexities while maintaining minimal uncertainties.

85   Currently, several in-house standards are being used as reference materials, including Duff

86   Brown Tank (64 Ma; Hill et al., 2016), and JT (13.797 ± 0.031 Ma; Guillong et al., 2020). The

87   only well-characterized reference material that is distributed across laboratories is the WC1

88   calcite with an age of 254.4 ± 6.5 2σs (2.5%) (Roberts et al., 2017). The use of WC1 alone for

89   mass-bias correction has several disadvantages. First, it is highly recommended with all in situ

90   U-Th-Pb geochronology to use secondary RMs to validate any correction parameters that are

91   being used, and to appropriately propagate uncertainties. Second, the relatively high

92   uncertainty (2.5%) on the age of WC1 sets a minimal uncertainty on any LA U-Pb age

93   determination. Finally, the quantity of the WC1 sample that is currently available for future

94   work is limited and is likely to not fully meet the growing demands of the LA scientific

95   community; although, we note here that there is a potential for further sample collection from

96   the original site.

97   This contribution introduces a new carbonate reference material that can be widely used for *in-*

98   *situ* dating of calcite as primary or as cross-reference material with other available standards.

99 We characterise the reference material at various resolutions using a combination of (1) laser

100 ablation imaging (20 µm square beam); (2) LA spot analysis, ~80-110 µm in diameter,

101 conducted on both single-collector and multi-collector (MC) ~~and single collector~~ inductively

102 coupled plasma mass spectrometer (ICP-MS); and (3) ID-TIMS analyses of ~~36~~ 37 sub-samples

103 (~1-7 mg aliquots). We discuss several key issues related to the use of ASH-15 sample as a

104 RM, including down-hole fractionation, heterogeneities, and previous bulk analyses~~, and the~~

105 ~~possible effect of samples size and blank corrections~~, to provide the best correction parameters

106 and suggested protocols for users of the LA scientific community.

107 **1 The ASH-15 flowstone**

108 The ASH-15 flowstone was found in Ashalim Cave, a karstic cave in the central Negev Desert

109 (30°56′36.2″ N, 34°44′22.5″ E), southern Israel, which is part of the northern margin of the

110 Saharan–Arabian desert belt. The cave entrance is located at an elevation of 414 m above sea

111 level and 67 km SE from the Mediterranean Sea coast. The cave is a three-dimensional

112 hypogene maze with a total length of 540 m, situated in Turonian limestone rock strata, at

113 depths of 0-31 m below the surface. The cave is richly decorated with vadose speleothems,

114 such as stalagmites, stalactites and flowstone, which are not active today because of the aridity

115 of the climate in the area (Vaks et al, 2010, 2018), but periods of their deposition correspond

116 to past episodes of wet climate in present-day desert. The thickness of the speleothems varies

117 from several cm to a few tens of cm. The soil above the cave is silicate loess, originated mainly

118 from aeolian dust (Crouvi et al., 2010) and the present day vegetation is composed of sparse

119 xeric shrubs with <10% vegetation cover.

120 The vadose speleothems of Ashalim Cave are composed of low-Mg calcite, and are divided

121 into a relatively thick Pliocene Basal layer, and thinner Pleistocene layers above it. The Basal

122 layer varies from 5 to 25 cm in thickness and comprises c. 90% of the speleothem volume in

123   the cave. It is composed of massive yellow calcite crystals (Fig. 1a-b), often showing

124   continuous growth in stalagmites and flowstone, suggesting deposition from continuously

125   dripping water. In all speleothems the Basal layer is terminated at its top by a <1 mm layer of

126   microcrystalline calcite, evaporite minerals and reddish clays (Fig. 1a), that is interpreted as a

127   hiatus (growth break) separating the Basal Pliocene layer and Quaternary layers above it (Vaks

128   et al., 2013). The thickness of Pleistocene top layers varies from several mm to 17 cm, but

129   usually does not exceed a few cm, comprising about 10% of the speleothem volume in the cave.

130   It is composed of alternating layers of brown calcite, with the youngest top layer (where found)

131   composed of yellow calcite. Several variably colored layers <1 mm thick of microcrystalline

132   calcite, evaporite minerals and reddish clays are found within the columnar crystalline structure,

133   suggesting hiatuses in speleothem deposition (Vaks et al., 2013).

134   The youngest periods of speleothem deposition in several Ashalim Cave speleothems were

135   dated by the ^{238}U-^{230}Th method and occurred from 221 ka to 190 ka and from 134 to 114 ka

136   (Vaks et al, 2010). Earlier periods of deposition were dated by the U-Pb method on ASH-15

137   flowstone ~~and are dated to~~at 1.272 ± 0.018 Ma (ASH-15-C), and the Basal layer of ASH-15

138   flowstone (layers D-K) ~~dated to~~at c. ~3.1 Ma (Fig 1a). These layers have been dated in three

139   different labs following several protocols for ID analysis (Vaks et al., 2013; Mason et al., 2013).

140   The U concentrations in speleothem calcite range between 1.9 and 19.7 µg/g and the amounts

141   of non-radiogenic Th are negligible (Vaks et al., 2010).
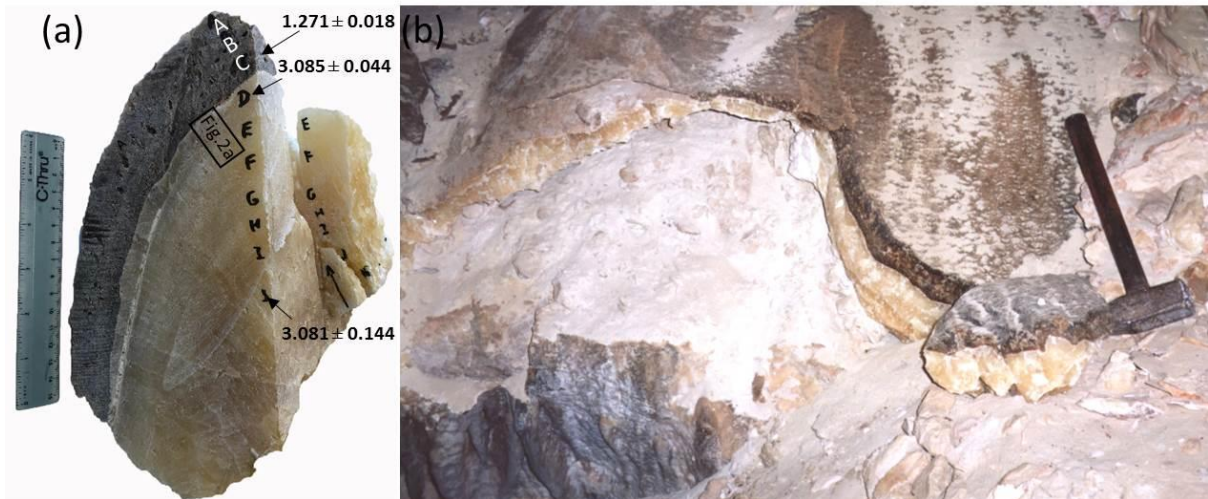
Figure 1. Sample ASH-15 from Ashalim Cave. (a) ~5 kg block of sample ASH-15 flowstone consisting of the massive Pliocene yellow Basal layer (>2 cm calcite crystals; section D–K) and the brown Quaternary layer (top section, A–C), the thin layer between the two stratigraphic members represents a growth break (hiatus). The main U-Pb ages of Vaks et al., 2013 are indicated; ~(b) In-situ flowstone within Ashalim Cave from which ASH-15 was sampled, showing the large reservoir of this flowstone.

2   Sample ASH-15 textural characterization

The ASH-15 thin-section includes section D and E ~~of the ASH-15 sample~~ (see location in Fig.1a). Overall the thin-section examination indicates that the original texture is preserved with consistent growth direction, no observed hiatus, and no indications for dissolution and recrystallization. A spot analysis array, 85 µm in diameter, targeted along growth ~~bands~~ zone and ~~perpendicular to~~along –growth direction ~~are~~ is visible in Fig. 2a-c. The ASH-15 sample shows no luminescence under cathodoluminescence light (Fig. 2c), suggesting formation under oxidising conditions. The slight bright luminescence observed within grain boundaries, discontinuities, and veins (arrows in Fig. 2b-c) may suggest ~~for~~ the presence of fluid inclusions, textural differences, or some local replacement within these areas. These areas should be

160   avoided if possible during spot analysis. The relatively homogenous low luminescence may

161   suggest for a single-phase continuous calcite growth, whereby precipitation occurred relatively

162   rapid from the same fluid source (e.g. with consistent Mn^{2+} Fe^{2+} composition) and/or under

163   similar precipitation redox conditions. This 15 cm thick, ~3 Ma Pliocene layer (section D-K)

164   is essentially of the same age. For this reason, previous dating of this sample also considered a

165   similar initial $^{234}U/^{238}U$ activity ratio for disequilibrium correction (Mason et al., 2013; Vaks

166   et al., 2013). The ASH-15 reference material consists of the whole Pliocene section that

167   terminates with a sharp transition to the darker Pleistocene layers above it (section A-C; see

168   Fig. 1b). About 3 kg of ASH-15 sample are excavated from the Ashalim Cave (Fig. 1a), and

169   potentially much more can be sampled in the future (we estimate more than 10 kg of sample;

170   Fig. 1b). The ASH-15 flowstone is therefore a good candidate for a reference material because

171   of its large volume, high U concentrations, and potentially homogenous age which will be

172   examine next.

173
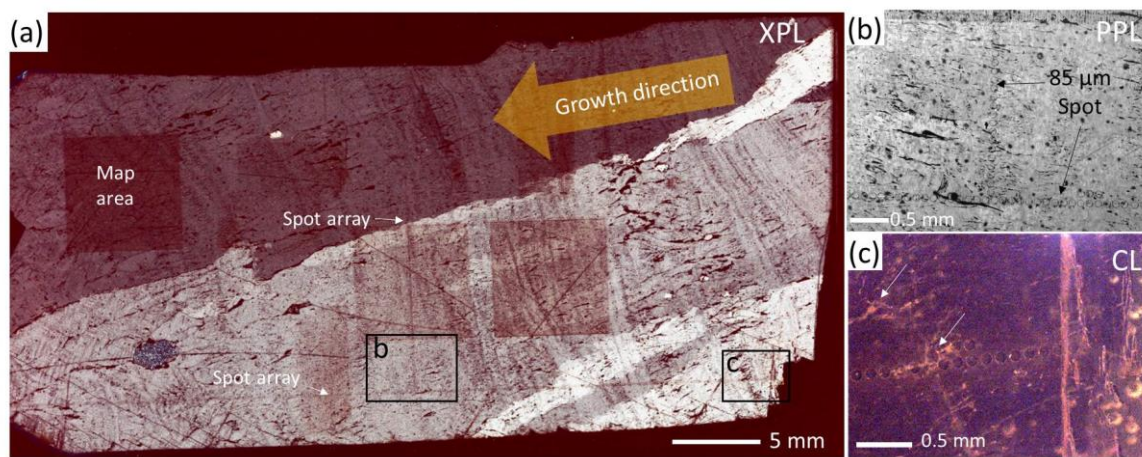
Figure 2. ASH-15D-E thin-section. (a) cross-polarized (XPL) scan ~~of ASH-15D-E thin-section~~,

175   36 mm long, showing continuous growth (no hiatus), and consistent growth direction (indicated

176   with yellow arrow). Spot analyses are targeted either sub-parallel to growth ~~band~~ zone or

177   ~~perpendicular~~ sub-parallel to growth direction; (b) close-up on spot array analyses (location is

178 shown in a) with 85 µm diameter; (c) CL image ~~of the same area~~ showing no luminescence

179 ~~and~~ except for some bright luminescence within grains boundaries and veins (arrows).

3   Methods

3.1   Elemental mapping

182 The sample ASH-15 was cut perpendicular to the growth ~~bands~~ zone of section D and E (see

183 Fig.1b) in order to examine heterogeneities across growth ~~bands~~ zone and within. Thin-sections

184 were then examined under plane- and cross-polarized light (XPL/PPL), and

185 cathodoluminescence (CL) microscopy (Fig. 2). The central part of the thin-section was also

186 analyzed for elemental distribution of selected elements. The elemental maps were measured

187 via LA-ICPMS, carried out on a 193 nm ArF excimer laser ablation system (Analyte G2

188 Teledyne Photon Machines Inc., Bozeman MT) coupled to an ICP-QMS (Agilent 7900, Agilent

189 Technologies, Santa Clara CA). The laser was equipped with a Photon Machines HelEx II

190 ablation chamber and an Aerosol Rapid Introduction System (ARIS). The experiments were

191 carried out using acquisition parameters (both on the ICP and on the laser) modelled using the

192 approach of van Elteren et al (2019; 2018) to avoid artefacts (e.g., aliasing, smear, blur). All

193 images (500x500 pixels) were acquired using a 20 µm square beam, fluence of 3.5 Jcm^{-2}, 294

194 Hz repetition rate and dosage of 10 (10 overlapping pulses per spot size which amount~~ing~~ to a

195 scanning speed of 588 µms^{-1}). The masses monitored were ~~^{24}Mg, ^{55}Mn, ^{63}Cu, ^{85}Rb~~ ^{88}Sr, ^{137}Ba,

196 ^{206}Pb, ^{208}Pb, ^{232}Th, and ^{238}U and the images were constructed using Photon Machines' HDIP

197 data reduction software (van Malderen, 2017).

3.2   LA-MC-ICPMS spot analyses

199 A thin section of ASH-15 was dated by U-Pb laser ablation multi-collector inductively coupled

200 plasma mass spectrometry (LA-MC-ICPMS) following the method described in Nuriel et al.

201 (2017). A Nu Plasma 3D was employed in conjunction with a Photon Machines Excite 193nm

202 Excimer laser equipped with a HelEex two volume cell. The laser was fired for 15 s during

203 analysis, using a ~~re~~repetition rate of 10 Hz, a spot size of 85 µm, and a fluence of approx. 1

204 J/cm^2. The Nu Plasma 3D allows for the simultaneous acquisition of ^{238}U, ^{235}U, ^{232}Th, ^{208}Pb,

205 ^{207}Pb, ^{206}Pb, ^{204}Pb(+Hg), and ^{202}Hg, where ^{238}U-^{232}Th are measured on Faraday detectors and

206 the low-side masses are measured on Daly detectors. Instrumental mass-bias was corrected

207 using a two-step approach: both the ^{207}Pb/^{206}Pb and ^{206}Pb/^{238}U ratios were first corrected to

208 NIST-614 glass reference material in *Iolite 3* using the geochronology reduction scheme (Paton

209 et al., 2010) to account for both mass-bias (^{207}Pb/^{206}Pb) and instrumental drift (^{207}Pb/^{206}Pb and

210 ^{206}Pb/^{238}U). The Tera-Wasserburg data, output from *Iolite*, was then plotted and ^{206}Pb/^{238}U

211 ratios of all RMs and unknowns were adjusted such that the primary calcite reference

212 material—WC-1—yielded an age of 254 Ma (Roberts et al., 2017). This resulted in accurate

213 dates for both our secondary calcite RM~~:~~, Duff Brown Tank at ~~–~~66.8 ± 3.4 Ma (previously

214 reported 64 Ma; Hill et al., 2016) and ~~a~~ a ^{207}Pb/^{206}Pb date of zircon RM at 566.0 ± 2.8 Ma

215 (previously reported~~Sri Lanka,~~ 564 Ma; Gehrels et al., 2008)~~, of 66.8 ± 3.4 Ma and a ^{207}Pb/^{206}Pb~~

216 ~~date of a 566.0 ± 2.8 Ma~~. Uncertainty propagation of individual ratios was assessed by

217 reproducibility of the NIST614 and SL RMs (n=44 in both cases) and added in quadrature such

218 that the MSWD of each weighted average is ≤1 and that the uncertainty is no better than 2%

219 (long-term reproducibility); this resulted in propagated uncertainties of 2.5% and 2% for the

220 ^{206}Pb/^{238}U and ^{207}Pb/^{206}Pb ratios, respectively. Given that the typical uncertainties of the

221 ^{206}Pb/^{238}U and ^{207}Pb/^{206}Pb ratios of the unknowns was >10% and >3%, respectively, the

222 uncertainty propagation on individual ratios had little effect on the calculation of the final date

223 of ASH-15. The thin section of ASH-15 was measured both parallel to the length of section

224 (303 spots, and perpendicular to it (101 spots). Data are plotted using Isoplot (Ludwig, 1998).

225

226

3.3 LA-ICPMS spot analyses

Analyses were conducted at the Geochronology and Tracers Facility, British Geological Survey (Nottingham, UK). The instrumentation comprised a New Wave Research 193UC excimer laser ablation system fitted with a TV2 cell, coupled to a Nu Instruments Attom single collector ~~inductively coupled plasma mass spectrometer~~ (ICP-MS~~)~~. The method follows the protocols described in Roberts and Walker (2016) and Roberts et al. (2017). Laser parameters varied slightly per session, but typically involve a pre-ablation cleaning spot of 150 µm, fired at 10 Hz with a fluence of ~6 J/cm^2 for 2 seconds, and ablation conditions of 80-100 µm spots, fired at 10 Hz with a fluence of ~6-8 J/cm^2 for 25-30 seconds. A 60 second background is taken before every set of standard-bracketed analyses, and a 5 second washout is left between each ablation. Normalization of Pb-Pb ratios is achieved using NIST614 glass (values of Woodhead and Hergt, 2001), and WC-1 carbonate for Pb-U ratios (Roberts et al., 2017). Data reduction uses the Time Resolved Analysis function of the Nu Instruments Attolab software, and an excel spreadsheet, with uncertainty propagation following the recommendations of Horstwood et al. (2016).

3.4 ID-TIMS U-Pb geochronology

Isotope dilution thermal ionization mass spectrometry (ID-TIMS) U-Pb geochronology was performed at the Institute of Geochemistry and Petrology of ETH Zurich (ETHZ) and at the Department of Earth Sciences of the University of Geneva (UNIGE). ~~Millimeter~~Millimetre-sized chips of the ASH-15-D and ASH-15-K calcite were extracted using stainless steel tools. Larger chips were further sub-divided resulting in ~1-7 mg aliquots. Individual chips were transferred into 3 ml Savillex beakers and repeatedly ultrasonically cleaned in ultrapure acetone and water. Cleaned sampled were transferred into pre-cleaned 3 ml Savillex beakers, spiked

251   with ~5-10 mg EARTHTIME (^{202}Pb-)^{205}Pb-^{233}U-^{235}U tracer solution (Condon et al., 2015) and

252   dissolved in 6N HCl at 120°C on a hotplate for ~30 minutes to assure complete dissolution and

253   sample-spike equilibration. Dissolved samples were dried down and redissolved in 1N HBr.

254   Uranium and Pb were separated using a single-column (50 µl, AG1-X8 resin) HBr-HCl anion

255   exchange chemistry. The Pb fraction was dried down with a drop of H_3PO_4 after a single

256   column pass. Uranium was dried down, redissolved in 3N HCl and further purified with a HCl-

257   based second column pass before drying it down with a drop of H_3PO_4. Uranium and Pb were

258   loaded on outgassed single Re filaments with ~1 µl of Si-gel emitter for thermal ionization

259   mass spectrometry. Uranium and Pb isotope ratios were measured on a Thermo TRITON Plus

260   at ETHZ and a Thermo TRITON at UNIGE. Lead isotopes were measured on the axial

261   secondary electron multiplier employing dynamic peak-hopping routine collecting masses

262   (202), 204, 205, 206, 207 and 208. Measured Pb isotope ratios were corrected for mass

263   fractionation either using the double spike (ETHZ) or using a mass fractionation factor of 0.15

264   ± 0.03 %/amu for single Pb spiked samples (UNIGE). Uranium isotope ratios were measured

265   as uranium-oxide (UO_2) employing a static measurement routine with Faraday cups connected

266   to amplifiers with 10^{13} ohm feedback resistors (von Quadt et al., 2016; Wotzlaw et al., 2017).

267   Isotope ratios were corrected for isobaric interferences from minor UO_2 isotopologues

268   (Wotzlaw et al., 2017) and for mass fractionation using the double spike assuming a ^{238}U/^{235}U

269   ratio of 137.818 ± 0.045 (Hiess et al., 2012) for sample and blank. Total procedural Pb blanks

270   for the HBr-based chemistry at ETHZ are consistently between 0.2 and 0.4 pg. We therefore

271   attribute up to 0.4 pg to laboratory blank with the remaining common Pb being attributed to

272   initial common Pb. Total procedural blanks measured at UNIGE yielded an average of 1.15 pg

273   that was taken as the laboratory blank contribution. Data reduction and uncertainty propagation

274   was performed using Tripoli and an Microsoft Excel-based spreadsheet that uses the algorithms

275   of Schmitz and Schoene (2007). Isochron calculations were performed using IsoplotR

276 (Vermeesch, 2018). All uncertainties are reported at 95% confidence ignoring systematic

277 uncertainties associated with the tracer calibration and decay constants unless otherwise stated.

4 Results

279 All analyses were performed on ASH-15-D-K yellow Pliocene layer, abbreviated here as

280 "ASH-15" unless specification of ASH-15-D, E etc. is indicated. The ASH-15-A-C brown

281 Pleistocene layer is not part of the ASH-15 suggested reference material.

4.1 LA elemental mapping

283 Elemental mapping for ^{88}Sr, ^{137}Ba, ^{206}Pb, ^{208}Pb, ^{238}U and ^{238}U/^{206}Pb ratio shows that the

284 distribution of most elements is relatively homogeneous (Fig.3), and in good accordance with

285 the luminescence data. Higher intensities for ^{238}U and ^{88}Sr were observed along grain

286 boundaries and discontinuities, whereas Pb and the rest of the trace elements are more

287 homogeneously distributed, arguing for steady environmental conditions that have kept steady

288 during the deposition. Ten random regions of interest (ROI) were selected throughout the

289 sample to mimic 10 spot analysis carried out at 85-90 microns spot size – just like one would

290 do for U-Pb geochronology, for example. These ROIs were generated by drawing on the map

291 circular regions with the radius of 85 or 90 microns in diameter. The pixels comprising each

292 ROI were pooled together as representing the equivalent of a single spot analysis. The statistical

293 data for each cluster (data are given in supplementary file) was were compared. The average

294 values for all pixel data is are within 2 standard errors and in good agreement, indicating that,

295 at least based on the elemental distribution we measured, the sample is relatively homogeneous

296 for a natural sample. To further investigate the chemical homogeneity of the sample, a random

297 transect through one of the growth zones was drawn and the signal intensities for ^{238}U were

298 extracted. The transect data also indicate that ^{238}U variations are within 2 standard errors of the

299 average value. (full data is available in Table S1 in the supplement).
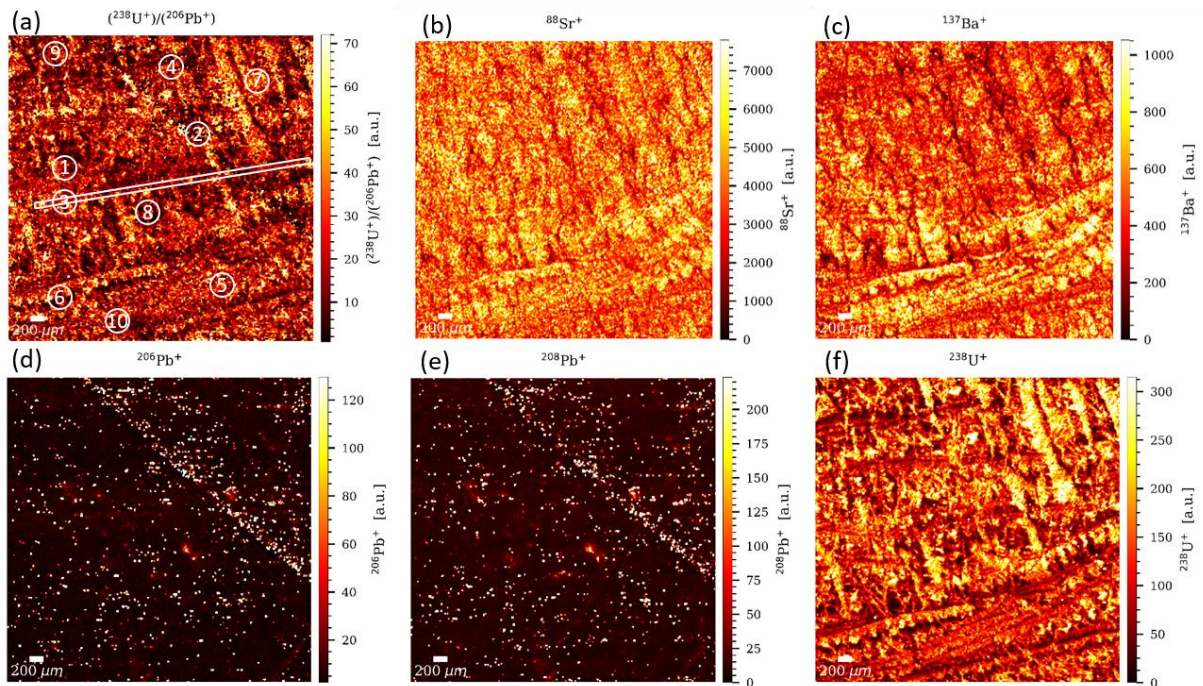
Figure 3. Signal intensity maps of ASH-15. Ffor ^{238}U/^{206}Pb, ^{88}Sr, ^{137}Ba, ^{206}Pb, ^{208}Pb, and ^{238}U

(a-d). The plotted signal was corrected for blank and analytical drift of the instrumentation.

Note that each distribution map has its own signal intensity scale. The position of the regions

of interest and transect is shown in (a). The circles designating the location of the regions of

interest are not at scale. (data is available in Table S1 in the supplement).

4.2 LA-MC-ICPMS spot analyses

Data and calculated ages for the LA-MC-ICPMS transects are shown in Tera-Wasserburg

space in Fig. 4 (n = 379 of 412 total spots). Analyses rejected from the age calculation include

those with ^{207}Pb/^{206}Pb uncertainties larger than 0.1% (n = 2) and those with high common-Pb

contents (^{208}Pb cps >5000; n = 17). A further 14 spots plotted below the array; these data were

represent the first 1–2 mm of spots of the lengthwise transect (lower right in Fig. 2a), and

suggest that a small percent of ASH-15 may behave differently during ablation and/or may

have been subsequently modified after crystallization; upon inspection, this portion of the

section contains more pore space and impurities than the majority of the section. The remaining

315   379 define a normally distributed array with a lower intercept age of 2.952 ± 0.043 Ma (MSWD

316   = 2.5), which is well within uncertainty of the new ID-TIMS data presented ~~herein~~ (full data is

317   available in Table S2 in the supplement)~~and the scatter observed in the LA data (i.e., MSWD~~

318   ~~> 1) is lower compared with scatter observed in the ID-TIMS data~~. The calculated upper

319   intercept of each transect is equivalent and within 1% of the common Pb composition

320   calculated from the ID-TIMS data. Not surprisingly, the lengthwise transect reveals a larger

321   spread in common/radiogenic Pb ratios; this transect crosses more growth zones and has a

322   higher probability of sampling a variety of concentrations of both Pb and U. Conversely, the

323   more limited spread in common/radiogenic Pb ratios appears to reflect the limited sampling of

324   growth zones, and would suggest that individual growth zones contain a relatively limited

325   range of concentrations in U and Pb. The slightly higher MSWD for the lengthwise transect

326   (2.7) relative to the growth zone transect (2.5) could also reflect these inherited compositional

327   differences during growth history, and a resulted "mixing" or "averaging" of different growth

328   phase along calcite continuous growth.

329   Variations of ASH-15 ages during 20 different runs (with 5-30 spot analysis in each) using

330   both ~~single (ICPMS) and~~single-collector and multi-collector (~~MC~~ ICP-MS~~)~~ are shown in Fig.

331   4b (full data is available in Tables S3-S5 in the supplement). The ages are calculated using

332   IsoplotR, not anchored to ~~0.8315~~specific common-lead, and are not corrected for

333   disequilibrium. Although there is a large scatter in the ages of the different runs the average

334   ages (marked ~~in~~ with black box~~thick lines~~) ~~are~~ plot~~ted~~ close to the new ID-TIMS ages, or are

335   slightly younger in age.

336
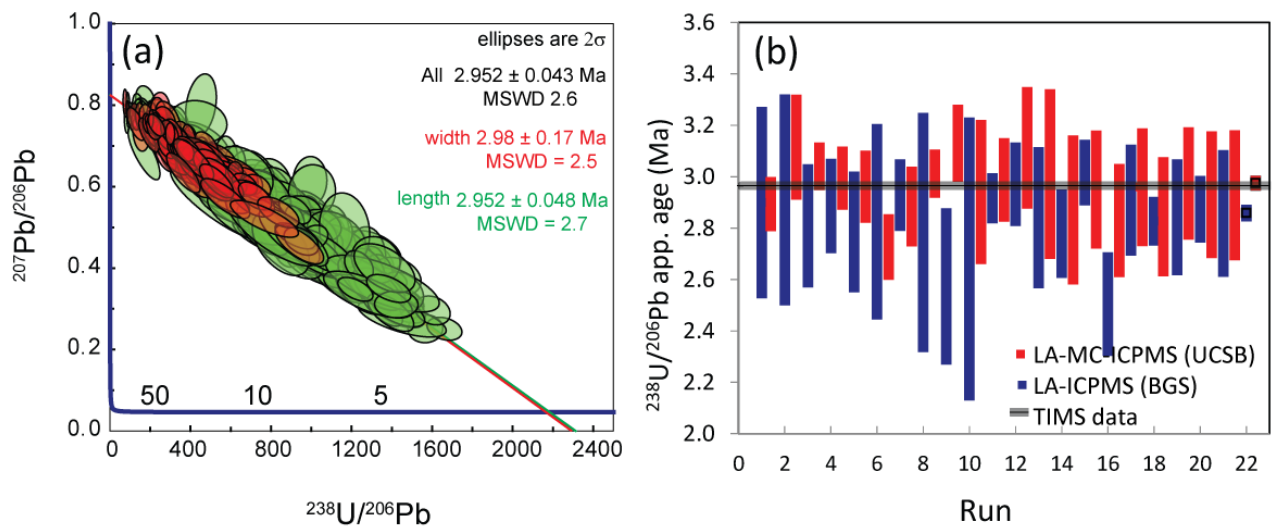
Figure 4. LA-MC-ICPMS analyses of calcite ASH-15. (a) Tera-Wasserburg concordia space plot (n=385) for (n=385). Spots spots analysis within lengthwise transect (green) and along growth zone transect (red). Calculated age, 2σ error and MSWD are given for both and for all spots together; (full data is available in Table S2 in the supplement); (b) Variations of ASH-15 ages during different runs using both single-collector (at the British Geological Survey) and multi-collector (at University of California Santa Barbara) ICP-MS. Ages are calculated using WC1 as primary MSRM; the new ID-TIMS age is indicated with a grey line; (full data is available in Table S3-S5 in the supplement) Ages are calculated using IsoplotR, anchored to 0.8315 common-lead, and are not corrected for disequilibrium.

4.3 Down-hole fractionation

Reference material is important for correction of both laser-induced elemental fractionation (LIEF) and in plasma-related ionization efficiency. Ideally, the reference material should resemble the unknown samples as much as possible in terms of its chemistry (e.g. Mg and Fe content), texture (i.e. micritic, crystalline), and age. The WC1 and ASH15 are both low-Mg calcite but they are very different in their textures and age. The ASH15 is a ~3 Ma, well-crystallized elongated calcite (up to 1 cm) and WC1 is a 254 Ma recrystallized botryoidal calcite, formed after aragonite. Despite these differences, both WC1 and ASH15 display a very

354 similar down-hole fractionation pattern (Fig. 5d). Fig. 5 shows stacked integration plots of the

355 down-hole raw ^{206}Pb/ ^{238}U ratio of different RMs including, the ASH15, WC-1, and Duff

356 Brown Tank (Black and Gulson, 1978). The ASH15 displays much larger scatter in the raw

357 data (Fig. 5a) in comparison to both WC1 and Duff Brown Tank (Fig. 5b-c), however, the

358 average value yielded identical down-hole ~~patterns~~ fractionation to that of WC-1 (Fig. 5d).

359 Duff Brown Tank is also consistent with the down-hole patterns b~~u~~et less steep in comparison

360 to WC1 and ASH15 (Fig. 5d). This comparison suggests that down-hole fractionation and

361 laser-induced elemental fractionation (LIEF) ~~is~~ are similar among the different RMs. It is thus

362 suggested that differences in measured and expected ^{206}Pb/^{238}U ratios ~~between measured and~~

363 ~~expected~~ in calcite material are likely to be caused mostly by plasma-ionization differences

364 between unknown samples and RMs.

365
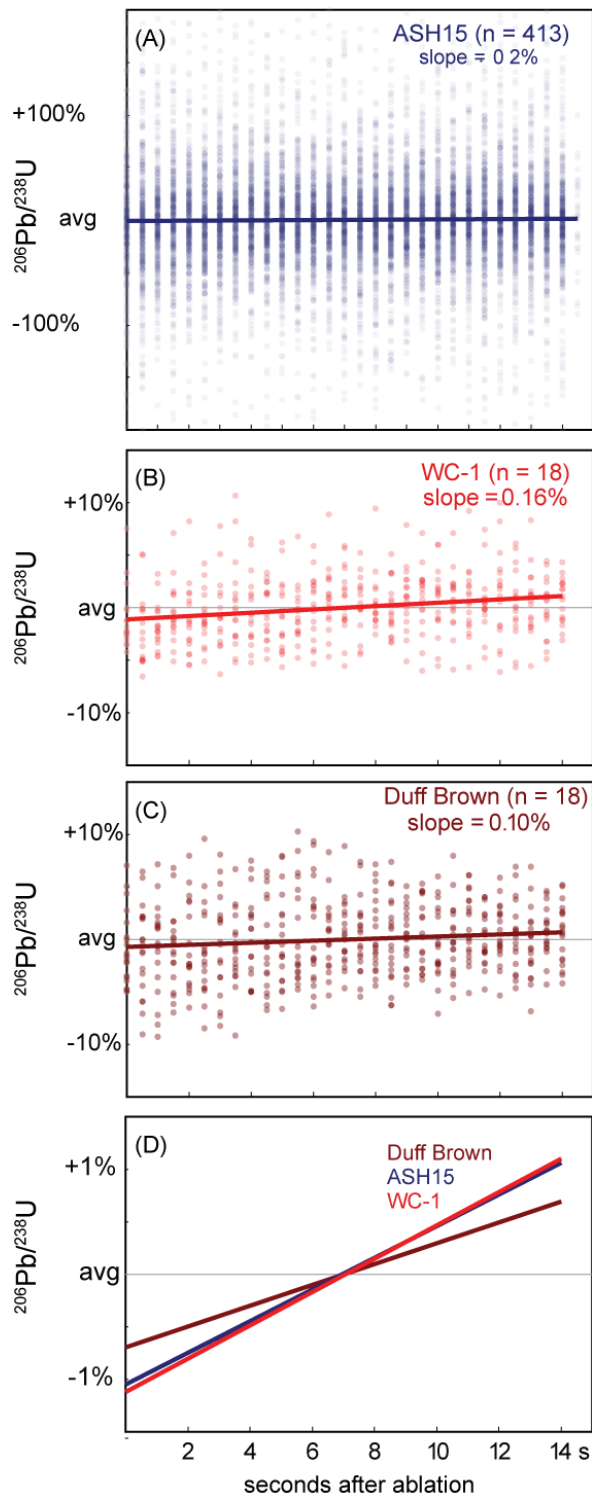
Figure 5. Stacked integration plots of raw [207]Pb-corrected [206]Pb/[238]U ratios for calcite reference

materials ASH-15, WC-1, and Duff Brown Tank. The low Pb concentration in ASH-15 yields

more scatter, but average slopes of all RMs are similar, with 1-2% change in age over 10

seconds (100 pulses) of ablation. The results suggest ~~for~~ minimal differences in down-hole

fractionation of the different RMs.

4.4 ID-TIMS results

Twelve aliquots of ASH-15D analyzed at ETHZ yielded $^{238}U/^{206}Pb$ ratios between 1096 and 2084 and $^{207}Pb/^{206}Pb$ ratios between 0.0825 and 0.4403 (full data is available in Table S6 in the supplement). Plotted in Tera-Wasserburg space, ~~this~~ these data ~~yields~~ yield a single isochron with an initial $^{207}Pb/^{206}Pb$ of 0.832 ± 0.015 (uncertainties are 95% confidence intervals) and a concordia intercept age of 2.967 ± 0.022 Ma (Fig. 6a). The elevated mean square weighted deviation (MSWD) of 12 is attributed to minor heterogeneities, most likely in the initial $^{207}Pb/^{206}Pb$ ratio of the speleothem calcite. Twelve aliquots of ASH-15K ~~analysed~~ analyzed at ETHZ returned $^{238}U/^{206}Pb$ ratios between 723 and 2094 and $^{207}Pb/^{206}Pb$ ratios between 0.0720 and 0.5677. In Tera-Wasserburg space, eleven out of twelve aliquots define a isochron with an initial $^{207}Pb/^{206}Pb$ of 0.8314 ± 0.0040 and a concordia intercept age of 2.964 ± 0.016 Ma (Fig. 6b). A single aliquot (#5.4) plots significantly below the isochron defined by the other aliquots. The elevated MSWD of 34 together with the single outlier suggest some heterogeneities in the initial $^{207}Pb/^{206}Pb$ of the ASH-15K calcite. Thirteen aliquots of ASH-15K ~~analysed~~ analyzed at UNIGE (pink color, Fig. 6b) yielded $^{238}U/^{206}Pb$ ratios between 433 and 1853 and and $^{207}Pb/^{206}Pb$ ratios ranging from 0.1856 to 0.6660. Twelve of the thirteen analyses yield ~~define~~ ~~an~~ best-fit ~~isochron~~ ~~isochron~~ line with an initial $^{207}Pb/^{206}Pb$ of 0.814 ± 0.019 and a Concordia intercept age of 2.947 ± 0.065 Ma. The elevated MSWD of 36 confirms the minor heterogeneity of the initial $^{207}Pb/^{206}Pb$.

The excellent agreement between the ASH-15D and ASH-15K datasets ~~suggest~~ indicates that the entire speleothem growth layer between these two growth zones is of equivalent age with minor heterogeneities in the initial $^{207}Pb/^{206}Pb$ ratio and justifies combining the data into a single isochron regression. The combined isochron, using 35 of 37 ~~analysed~~ analyzed aliquots, yields an initial $^{207}Pb/^{206}Pb$ of 0.8306 ± 0.0033 and a concordia intercept age of 2.965 ± 0.011

395   Ma with a MSWD of 35 (Fig. 6c). We consider the results of the combined ~~isochron~~ regression

396   as the best reference value for using ASH-15 as a primary reference material.

397   The new TIMS data provide the most extended bulk investigation ~~analyses work~~ of the ASH-

398   15 sample, with a total of 37 sub-samples that are separated from bottom (K, n=25) to top (D,

399   n=12) ~~sections of the sample~~. The ~~relatively~~ high MSWD of 35 is suggested to reflect true

400   heterogeneities of the dated material, possibly related to impurities that are concentrated within

401   grain boundaries (as suggested by CL and elemental mapping). We re-calculated previously

402   determined isochron ages of Vaks et al. (2013) and Mason et al. (2013; Fig. 7). We obtained

403   concordia intercept ages of 3.0088 ± 0.053 Ma for ASH-15-D (MSWD=11; n=5) and 3.0153

404   ± 0.042 Ma for ASH-15-K (MSWD=14; n=5) of Vaks et al. (2013) and 3.0015 ± 0.029 for

405   ASH-15-D (MSWD=2; n=5) of Mason et al. (2013). These ages ~~are systematically older but~~

406   ~~still overlap within uncertainty with~~ are largely overlapping within uncertainty with our new

407   ID-TIMS age of 2.965 ± 0.011 Ma (Fig. 7; and data in Table S7 in the supplements). The

408   apparent minor systematic offset towards slightly older ages is attributed to the lower number

409   of aliquots in the MC-ICPMS datasets combined with the heterogeneous initial Pb isotope

410   composition. ~~We speculate that the small but systematic offset between previous results and~~

411   ~~our new data may be related to natural heterogeneities that are sampled differently depending~~

412   ~~on sample size but we cannot exclude analytical differences as an additional source of bias.~~

413   ~~The origin of this bias between the two techniques should be investigated more systematically~~

414   ~~in future.~~ For laser ablation U-Pb work, we recommend the use of the new ID-TIMS age

415   because of the large number of sub-samples (n=37), and the small aliquots (1-7 mg) that are

416   more representative of laser-ablation spot analysis. In addition, the use of the precisely and

417   accurately calibrated EARTHTIME tracer solutions (Condon et al., 2015) and the online mass

418   fractionation correction provided by the double Pb and double U tracer are an important

419   advantage of this method ~~compared to previous bulk analyses~~. The excellent interlaboratory

420 reproducibility gives us additional confidences that our ID-TIMS data provide the most

421 accurate characterization of the U-Pb systematics of the ASH-15 calcite for use as a primary

422 reference material.
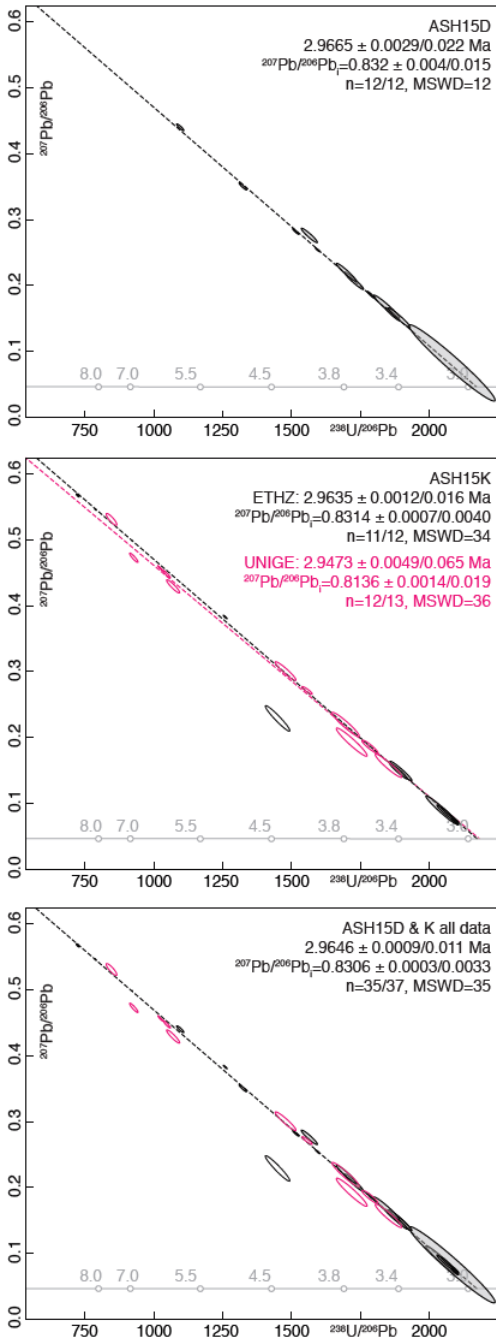
423

424 **Figure 6.** ID-TIMS U-Pb results for ASH-15D, ASH-15K, and for both ASH-15D–+K

425 displayed in Tera-Wasserburg concordia space. Uncertainties on the initial $^{207}Pb/^{206}Pb$ ratios

426 and the intercept ages are ~~given~~ reported at 95% confidence ~~as σ and as 95% confidence~~

427 ~~intervals~~ including overdispersion (Vermeesch, 2018).
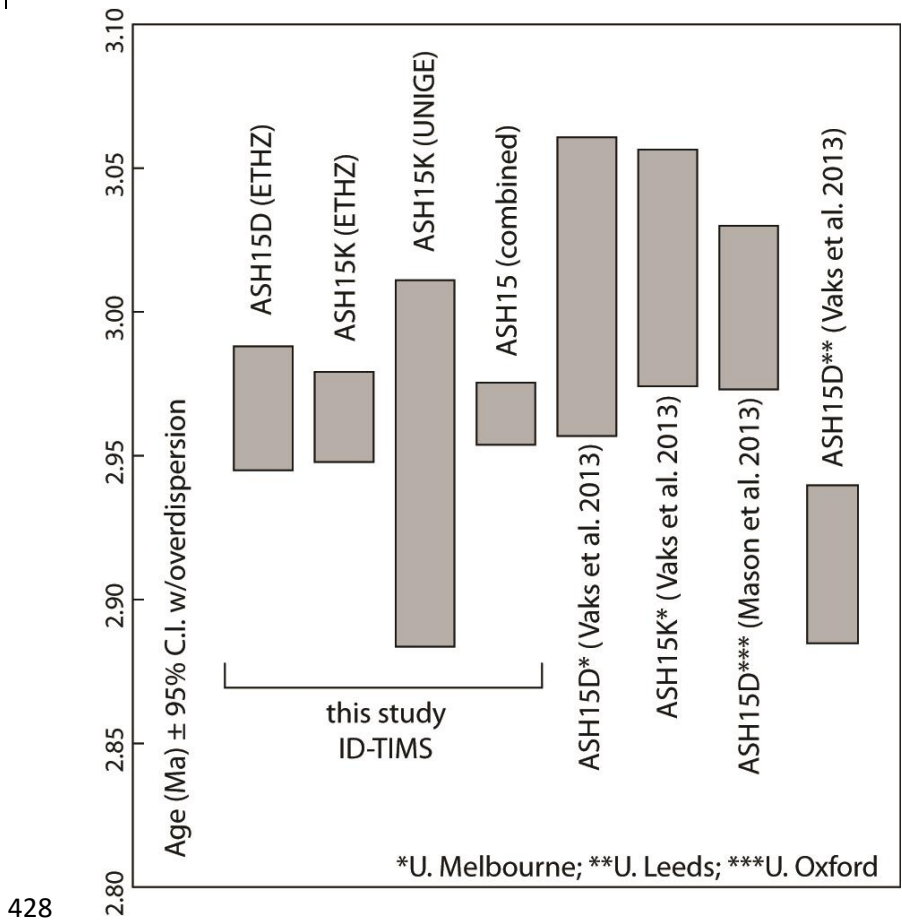
Figure 7. Previous (re-calculated) and new ages of ASH-15 from isotope-dilution U-Pb

analysis. All ages are calculated using IsoplotR (Vermeesch, 2018), ~~and~~ are not corrected for

disequilibrium and are not anchored to common-lead specific value (see data in Table S7 in

the supplements).

4.5   Calcite reference material

The U and Pb concentrations of carbonate materials vary greatly. Data compilation by Roberts

et al. (2020; this issue) combined hundreds of carbonate samples from different origin such as

diagenetic, biogenic, speleothem, and vein-fill. This compilation indicates several orders of

magnitude differences in U and Pb concentrations of the different types of carbonate and the

heterogeneity of spot analysis within each type or even a single sample. A modified

representation of their data, excluding calcite vein-fill, which vary throughout the entire

compositional range, is shown together with the currently available calcite reference materials

(Fig. 8; and full data in Table S8 in the supplement). Note that both ASH15 and JT, display

much larger heterogeneity when measured by LA-ICPMS (small symbols) relative to ID-TIMS

(large symbols). Despite the high compositional heterogeneity of each of the reference material,

they show minimal overlap and together they cover most of the compositional range of the

presented carbonate material. WC1 (Roberts et al., 2017) with relatively high U and Pb

concentrations can easily be measured on less-sensitive ICP-MS such as quadrupole

instruments, and is most appropriate to be used for dating vein-fill and diagenetic carbonates.

In contrast, the ASH15 flowstone, with relatively low Pb and high U concentration that are

better measured on more-sensitive ICP-MS (e.g. new generation of single-collector and multi-

collector ICP-MS), and is most appropriate for dating speleothem type carbonates. Finally the

JT (Guillong et al., 2020), with moderate U and Pb concentration can be used can be used for

most single- collector and multi-collector sector-field ICP-MS instrument as well as the newer

generation of quadrupole ICP-MS. Reference material with high Pb and low U or both low U

and Pb concentrations will further help to cover the full compositional range of carbonate

material but may introduce analytical challenges.
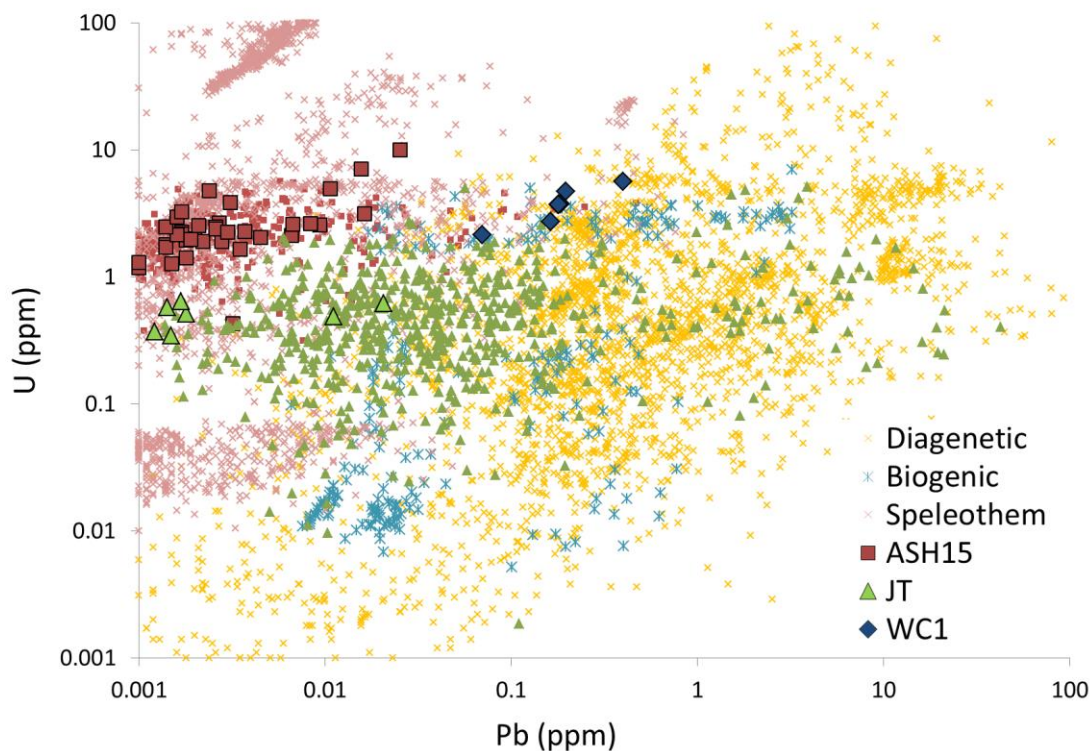
Figure 8. U and Pb concentrations of different carbonate samples and available reference materials. Large and small symbols for the reference materials indicate ID-TIMS and LA-ICPMS analyses, respectively. Note the minimal compositional overlap of the three reference materials (ASH15, WC1, and JT). Data for diagenetic, biogenic, and speleothem carbonates are from Roberts et al. (2020, this issue). Data for JT standard are from Guillong et al. (2020).

5 Conclusions

The ASH-15 speleothem calcite is characterized as a matrix matched reference material for LA-ICPMS U-Pb geochronology of calcite. ID-TIMS analyses of small 1-7 mg aliquots of two growth zones suggest sufficient homogeneity with a combined intercept age of 2.965 ± 0.011 Ma and an initial $^{207}Pb/^{206}Pb$ of 0.8315 ± 0.0026. These data are recommended as the reference values for the ASH-15 calcite reference material. The excellent agreement between the two growth zones suggest that the entire interval between the two dated layers can be used with the same reference age. Compared to other calcite reference material (e.g. WC1), ASH-15 is more

472 homogeneous but has lower radiogenic Pb content and therefore requires more sensitive

473 instruments (i.e. sector field rather than quadrupole mass spectrometers) to be used as a

474 reference material.

475

476 **Author's contribution**

477 PN: data processing and writing, JFW: ID-TIMS analysis and writing, MO: ID-TIMS

478 analysis, AV: sample collection and writing, CS: LA mapping analysis and writing, MS: LA

479 mapping analysis. NR: LA-ICPMS, data analysis and writing. AKC: LA-MC-ICPMS, data

480 analysis and writing.

481

482 **Competing interests**

483 The authors declare that they have no conflict of interest.

484

485 **Acknowledgements**

486 We thank reviewers Fernando Corfu and Jon Woodhead as well as editor Axel Gerdes for

487 constructive comments and suggestions. We thank Bar Elisha for thin-section preparation and

488 to Andrew Mason for constructive discussion. This study was funded by the Israel Science

489 Foundation, Grant ISF-727/16.

Appendices
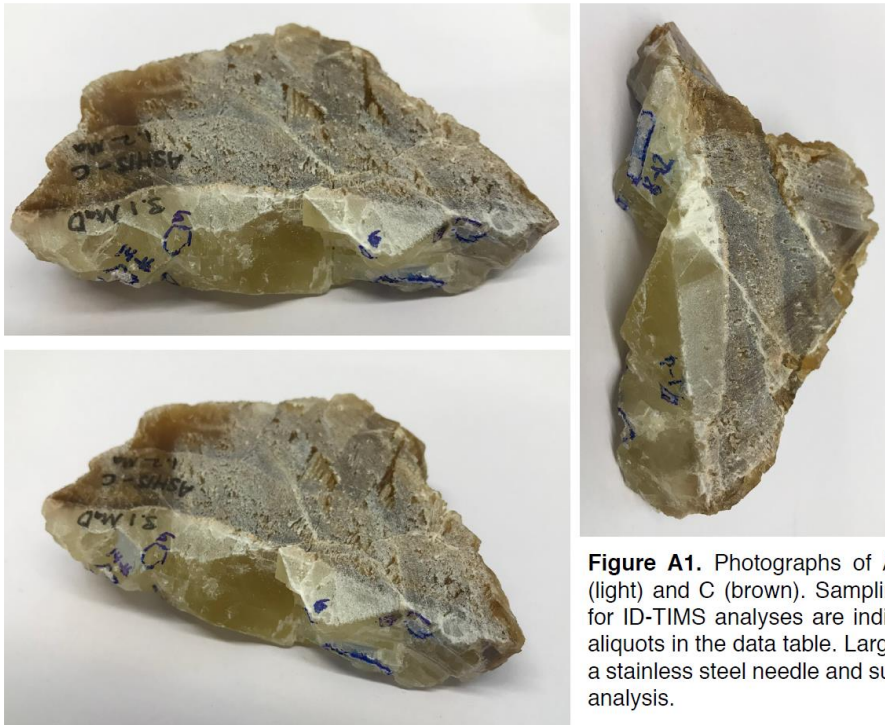
Figure A1. Photographs of ASH15 flowstone with layers D (light) and C (brown). Sampling localities of aliquots sampled for ID-TIMS analyses are indicated by numbers matching the aliquots in the data table. Larger pieces were chipped off using a stainless steel needle and subdivided into smaller aliquots for analysis.

Figure A2. Photographs of ASH15 flowstone with layers K (bottom) to D (top). Sampling localities of aliquots samples for ID-TIMS analyses within layer K are indicated with numbers (n=12) and are matching the aliquots in the data table.

References:

Anjiang, S., Anping, H., Cheng, T., Liang, F., Wenqing, P., Yuexing, F., and Zhao, J.: Laser ablation in situ U-Pb dating and its application to diagenesis-porosity evolution of carbonate reservoirs, 46, 1127-1140, 2019.

Condon, D., Schoene, B., McLean, N., Bowring, S., and Parrish, R.: Metrology and traceability of U–Pb isotope dilution geochronology (EARTHTIME Tracer Calibration Part I), Geochimica et Cosmochimica Acta, 164, 464-480, 2015.

Coogan, L. A., Parrish, R. R., and Roberts, N. M.: Early hydrothermal carbon uptake by the upper oceanic crust: Insight from in situ U-Pb dating, Geology, 44, 147-150, 2016.

Crouvi, O., Amit, R., Enzel, Y., and Gillespie, A. R.: Active sand seas and the formation of desert loess, Quaternary Science Reviews, 29, 2087-2098, 2010.

Godeau, N., Deschamps, P., Guihou, A., Leonide, P., Tendil, A., Gerdes, A., Hamelin, B., and Girard, J.-P. J. G.: U-Pb dating of calcite cement and diagenetic history in microporous carbonate reservoirs: Case of the Urgonian Limestone, France, 46, 247-250, 2018.

Goodfellow, B. W., Viola, G., Bingen, B., Nuriel, P., and Kylander-Clark, A. R. C.: Palaeocene faulting in SE Sweden from U–Pb dating of slickenfibre calcite, Terra Nova, n/a-n/a, 10.1111/ter.12280, 2017.

Guillong, M., Wotzlaw, J. F., Looser, N., and Laurent, O.: New analytical and data evaluation protocols to improve the reliability of U-Pb LA-ICP-MS carbonate dating, Geochronology Discuss., 2020, 1-17, 10.5194/gchron-2019-20, 2020.

Hansman, R. J., Albert, R., Gerdes, A., and Ring, U.: Absolute ages of multiple generations of brittle structures by U-Pb dating of calcite, Geology, 46, 207-210, 2018.

Hiess, J., Condon, D. J., McLean, N., and Noble, S. R.: 238U/235U systematics in terrestrial uranium-bearing minerals, Science, 335, 1610-1614, 2012.

Holdsworth, R., McCaffrey, K., Dempsey, E., Roberts, N., Hardman, K., Morton, A., Feely, M., Hunt, J., Conway, A., and Robertson, A.: Natural fracture propping and earthquake-induced oil migration in fractured basement reservoirs, Geology, 47, 700-704, 2019.

Horstwood, M. S., Košler, J., Gehrels, G., Jackson, S. E., McLean, N. M., Paton, C., Pearson, N. J., Sircombe, K., Sylvester, P., and Vermeesch, P.: Community-derived standards for LA-ICP-MS U-(Th-)Pb geochronology–Uncertainty propagation, age interpretation and data reporting, Geostandards and Geoanalytical Research, 40, 311-332, 2016.

Li, Q., Parrish, R., Horstwood, M., and McArthur, J.: U–Pb dating of cements in Mesozoic ammonites, Chemical Geology, 376, 76-83, 2014.

MacDonald, J., Faithfull, J., Roberts, N., Davies, A., Holdsworth, C., Newton, M., Williamson, S., Boyce, A., John, C. J. C. t. M., and Petrology: Clumped-isotope palaeothermometry and LA-ICP-MS U–Pb dating of lava-pile hydrothermal calcite veins, 174, 63, 2019.

Mason, A. J., Henderson, G. M., and Vaks, A.: An Acetic Acid-Based Extraction Protocol for the Recovery of U, Th and Pb from Calcium Carbonates for U-(Th)-Pb Geochronology, Geostandards and Geoanalytical Research, 37, 261-275, 10.1111/j.1751-908X.2013.00219.x, 2013.

Nuriel, P., Weinberger, R., Kylander-Clark, A. R. C., Hacker, B. R., and Craddock, J. P.: The onset of the Dead Sea transform based on calcite age-strain analyses, Geology, *45*, 587-590, 10.1130/g38903.1, 2017.

Nuriel, P., Craddock, J., Kylander-Clark, A. R., Uysal, I. T., Karabacak, V., Dirik, R. K., Hacker, B. R., and Weinberger, R. J. G.: Reactivation history of the North Anatolian fault zone based on calcite age-strain analyses, 47, 465-469, 2019.

Parrish, R. R., Parrish, C. M., and Lasalle, S.: Vein calcite dating reveals Pyrenean orogen as cause of Paleogene deformation in southern England, Journal of the Geological Society, 10.1144/jgs2017-107, 2018.

Piccione, G., Rasbury, E. T., Elliott, B. A., Kyle, J. R., Jaret, S. J., Acerbo, A. S., Lanzirotti, A., Northrup, P., Wooton, K., and Parrish, R. R.: Vein fluorite U-Pb dating demonstrates post–6.2 Ma rare-earth element mobilization associated with Rio Grande rifting, Geosphere, 15, 1958-1972, 2019.

Ring, U., and Gerdes, A.: Kinematics of the Alpenrhein-Bodensee graben system in the Central Alps: Oligocene/Miocene transtension due to formation of the Western Alps arc, Tectonics, 35, 1367-1391, 10.1002/2015TC004085/abstract, 2016.

Roberts, N. M., and Walker, R. J.: U-Pb geochronology of calcite-mineralized faults: Absolute timing of rift-related fault events on the northeast Atlantic margin, Geology, 44, 531-534, 2016.

Roberts, N. M., Rasbury, E. T., Parrish, R. R., Smith, C. J., Horstwood, M. S., and Condon, D. J.: A calcite reference material for LA-ICP-MS U-Pb geochronology, Geochemistry, Geophysics, Geosystems, 2017.

Roberts, N. M. W., Drost, K., Horstwood, M. S. A., Condon, D. J., Chew, D., Drake, H., Milodowski, A. E., McLean, N. M., Smye, A. J., Walker, R. J., Haslam, R., Hodson, K., Imber, J., Beaudoin, N., and Lee, J. K.: Laser ablation inductively coupled plasma mass spectrometry (LA-ICP-MS) U–Pb carbonate geochronology: strategies, progress, and limitations, Geochronology, 2, 33-61, 10.5194/gchron-2-33-2020, 2020.

Schmitz, M. D., and Schoene, B.: Derivation of isotope ratios, errors, and error correlations for U-Pb geochronology using 205Pb-235U-(233U)-spiked isotope dilution thermal ionization mass spectrometric data, Geochemistry, Geophysics, Geosystems, 8, 2007.

Vaks, A., Bar-Matthews, M., Matthews, A., Ayalon, A., and Frumkin, A.: Middle-Late Quaternary paleoclimate of northern margins of the Saharan-Arabian Desert: reconstruction from speleothems of Negev Desert, Israel, Quaternary Science Reviews, 29, 2647-2662, 2010.

Vaks, A., Woodhead, J., Bar-Matthews, M., Ayalon, A., Cliff, R. A., Zilberman, T., Matthews, A., and Frumkin, A.: Pliocene–Pleistocene climate of the northern margin of Saharan–Arabian Desert recorded in speleothems from the Negev Desert, Israel, Earth and Planetary Science Letters, 368, 88-100, http://dx.doi.org/10.1016/j.epsl.2013.02.027, 2013.

van Elteren, J. T., Šelih, V. S., Šala, M., Van Malderen, S. J., and Vanhaecke, F.: Imaging artifacts in continuous scanning 2D LA-ICPMS imaging due to nonsynchronization issues, Analytical chemistry, 90, 2896-2901, 2018.

van Elteren, J. T., Šelih, V. S., and Šala, M.: Insights into the selection of 2D LA-ICP-MS (multi) elemental mapping conditions, Journal of Analytical Atomic Spectrometry, 34, 1919-1931, 2019.

van Malderen, S.: Optimization of methods based on laser ablation-ICP-mass spectrometry (LA-ICP-MS) for 2-D and 3-D elemental mapping, Ghent University, 2017.

573   Vermeesch, P.: IsoplotR: A free and open toolbox for geochronology, Geoscience Frontiers, 2018.

574   von Quadt, A., Wotzlaw, J.-F., Buret, Y., Large, S. J., Peytcheva, I., and Trinquier, A.: High-precision
575   zircon U/Pb geochronology by ID-TIMS using new 10 13 ohm resistors, Journal of Analytical Atomic
576   Spectrometry, 31, 658-665, 2016.

577   Woodhead, J., and Petrus, J. J. G.: Exploring the advantages and limitations of in situ U–Pb carbonate
578   geochronology using speleothems, 1, 69-84, 2019.

579   Woodhead, J. D., and Hergt, J. M.: Strontium, neodymium and lead isotope analyses of NIST glass
580   certified reference materials: SRM 610, 612, 614, Geostandards Newsletter, 25, 261-266, 2001.

581   Wotzlaw, J.-F., Buret, Y., Large, S. J., Szymanowski, D., and von Quadt, A.: ID-TIMS U–Pb
582   geochronology at the 0.1‰ level using 10 13 Ω resistors and simultaneous U and 18 O/16 O isotope
583   ratio determination for accurate UO 2 interference correction, Journal of Analytical Atomic
584   Spectrometry, 32, 579-586, 2017.

585